Unraveling on kinesin acceleration in intracellular environments: A theory for active bath

Mengkai Feng and Zhonghuai Hou [*]

Hefei National Research Center for Physical Sciences at the Microscale & Department of Chemical Physics,
University of Science and Technology of China, Hefei, Anhui 230026, China

A single-molecular motor kinesin harnesses thermal and nonthermal fluctuations to transport various cargoes along microtubules, converting chemical energy to directed movements. To describe the nonthermal fluctuations generated by the complex environment in living cells, we propose a bottom-up model which combines a Markov model of the kinesin and a mean-field model for the active bath, to mimic the kinesin movements in the intracellular environment. Simulations of the model system show that the kinesin and the probe attached to it are accelerated by such active bath. Further, we provide a theoretical insight into the simulation result by deriving a generalized Langevin equation (GLE) for the probe with a mean-field method, wherein an effective friction kernel and fluctuating noise terms are obtained explicitly. Numerical solutions of the GLE show very good agreement with simulation results. We sample such noises, calculate their variances and non-Gaussian parameters, and reveal that the dominant contribution to probe acceleration is attributed to noise variance.

I. INTRODUCTION

Kinesins are a class of molecular motor proteins that are driven by hydrolysis of adenosine triphosphate (ATP) and move along microtubule filaments to transport various cargoes [1–3]. The kinetic mechanism of kinesin movement has been well studied through single-molecule measurement technologies [4–6]. Beyond direct ATP propulsion, in living cells, cargo-loaded kinesin utilizes thermal fluctuations to make directed motions [3,7]. Besides, metabolic activities, which are hard to recur in experimental conditions (*in vitro*) but do occur in living cells, generate nonthermal fluctuations through energy input [8–12]. A few works showed that active fluctuations have non-Gaussian properties in various physical systems, such as active swimmer suspensions [13–15] and cytoskeleton networks [16]. Effects of these active fluctuations have become a hot topic recently in biophysics and nonequilibrium statistical physics communities [13,17–19], and direct measurement of kinesin with nonthermal noises has been achieved experimentally (*in vitro*) [17,18,20].

It has been shown that active fluctuations promote the transport of molecular motors as far as we know [11,13,16–18,20,21]. Ariga *et al.* [17] studied the noise-induced acceleration of kinesin with experiments and a phenomenological theory. They found that kinesin accelerates under a semitruncated Lévy noise, and when a large hindering force is loaded, this acceleration becomes more significant. They also pointed

out that the efficiency of kinesin is surprisingly low *in vitro* [19] so that they hypothesized the kinesin movement is likely to be optimized for noisy intracellular environments but not necessarily for extracellular situations. Similarly, another class of motor proteins, dynein, also exhibits analogous behavior. Ezber *et al.* [21] found that dynein harnesses active fluctuations for faster movement experimentally, and described this phenomenon with a racket potential model based on Arrhenius theory. Analogously, Pak *et al.* [20] studied probe transport and diffusion enhancement in the ratchet potential and the presence of "exponentially correlated Poisson (ECP) noise" experimentally. They found that the probe velocity not only increased with noise strength, but also reached the maximum for a characteristic correlation timescale and non-Gaussian distribution of such noise.

On the other hand, when biological swimmers or artificial self-propelled particles are suspended in the fluid, the transport properties of the probe can be dramatically altered. This constitutes a model called "active bath" or "active suspension" that has been widely investigated experimentally and theoretically in recent decades [22–36]. In particular, significant progress has been made in recent years in modeling and theoretical research, which are based on various theoretical methods, including density functional theory [37], nonequilibrium linear response theory [29,38–43], mean-field theory method (including our previous work on the effective mobility and diffusion of a passive tracer in the active bath [44]) [45–50], and even mode-coupling theory [51,52]. The "active bath" model brings an available tool to investigate the probe properties in complex fluids which are far from equilibrium and evolve complicated interactions, such as cytoplasm in living cells. All these works inspire us to build a bottom-up model for kinesin in an intracellular environment and derive a corresponding theory that serves as a fundamental way to decode the kinesin acceleration in nonequilibrium situations.
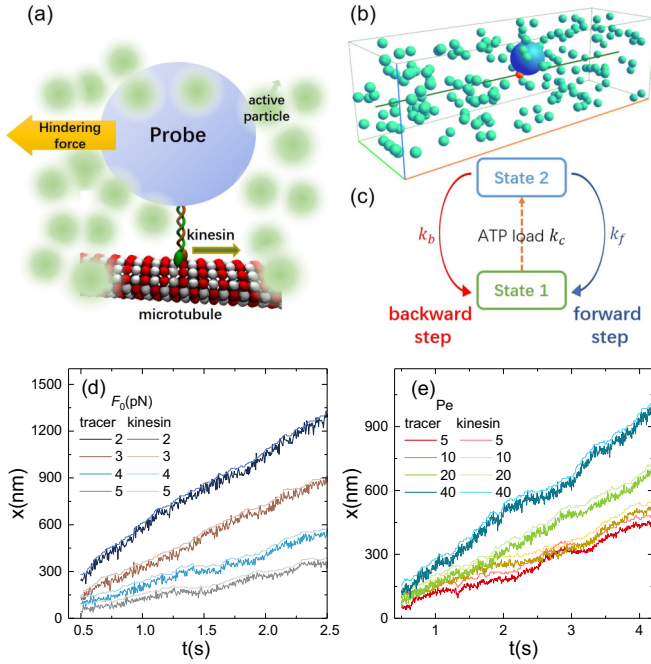
[*]hzhlj@ustc.edu.cn

FIG. 1. (a) Cartoon for the model system. (b) Schema for actual simulation system: Large blue ball stands for the probe, small cyan balls indicate active particles (only a few particles are shown), and red dots indicate the kinesin. (c) Schematic diagram for Markov model of kinesin movement. Typical trajectories of tracer and kinesin in the active bath (d) for different hindering forces from -2 to -4 pN with constant activity Pe $= 40$, and (e) for the different activity of bath under constant drag force $F_0 = -4$ pN.

In the present work, we introduce an active bath model to mimic the cytoplasmic environment, by utilizing soft colloidal particles (also known as "active crowders") to imitate various proteins or vesicae, and particle activity to simulate metabolic processes. Then we investigate the effects of thermal/nonthermal fluctuation generated by these crowders on kinesin transport. Our model briefly captures the most significant parts of the system and allows a wide range of parameters to include various kinds of situations. It brings a quantifiable research approach to active fluctuations in living cells.

II. MODELING AND SIMULATIONS

Let us consider a three-dimensional system shown in Fig. 1(a), where a probe (or called tracer elsewhere) attached to a kinesin is suspended in an active bath consisting of N self-propelled particles inside a box of side length L_x, L_y, L_z with periodic boundaries. These bath particles are propelled by independent Ornstein-Uhlenbeck (OU) noises, forced by interparticle repulsive potentials and background thermal noises. The movement of bath particles is governed by overdamped Langevin equations

$$\dot{\mathbf{r}}_i = -\mu_b \nabla_i \left[\sum_{j \neq i} V(|\mathbf{r}_i - \mathbf{r}_j|) + U(|\mathbf{r}_i - \mathbf{x}_p|) \right]$$

$$+ \mathbf{f}_i + \sqrt{2\mu_b k_B T} \boldsymbol{\xi}_i, \quad (1a)$$

$$\tau_b \dot{\mathbf{f}}_i = -\mathbf{f}_i + \sqrt{2D_b} \boldsymbol{\zeta}_i, \quad (1b)$$

where $\mathbf{r}_i$ is the position for the ith bath particle, μ_b is the mobility, $\mathbf{x}_p$ is the position of the probe particle, $V(r)$ and $U(r)$ are interacting potentials between bath-bath particles and bath-probe, respectively, $\mathbf{f}_i$ is the propulsion velocity acting on i-bath particles with persistent time τ_b and strength D_b, k_B is the Boltzmann constant and T is the background temperature, and $\boldsymbol{\xi}_i$ and $\boldsymbol{\eta}_i$ are independent Gaussian white noise vectors in 3d space, with zero means and delta correlations $\langle \boldsymbol{\xi}_i(t)\boldsymbol{\xi}_j(t') \rangle = 2\delta_{ij}\delta(t - t')\mathbf{I}$ and $\langle \boldsymbol{\zeta}_i(t)\boldsymbol{\zeta}_j(t') \rangle = 2\delta_{ij}\delta(t - t')\mathbf{I}$, where $\mathbf{I}$ is the unit matrix.

The molecular motor is described by a phenomenological Markov-like kinetic diagram based on experimental observations [19], wherein the complex kinesin walking process is simplified to a two-state Markov transition. In this model, the central ATP hydrolysis and the walking process are divided into three transition steps [see Fig. 1(c)]. The first step is ATP load with the constant rate k_c and causes a "state transition" (state 1 to state 2). This rate is dependent on the concentration of ATP, and independent of any mechanical issues. The second and third steps are mechanical transitions for forward and backward steps with constant step size $d = 8$ nm along the microtubule as well as rates k_f and k_b, respectively. Meanwhile, the state transition accompanies both steps, from state 2 to state 1. These two rates have both force F dependent as Arrhenius type

$$k_{\{f,b\}}(F) = k_{\{f,b\}}^0 \exp\left(\frac{d_{\{f,b\}}F}{k_B T}\right), \quad (2)$$

where $k_{\{f,b\}}^0$ is the rate constant without any external force load, $d_{\{f,b\}}$ is the characteristic distance, and all of these parameters are fitted by experimental data. Mathematically, the evolution of the probability of each state (P_1 and P_2) obeys a master equation

$$\frac{d}{dt}P_2 = k_c P_1 - (k_f + k_b)P_2. \quad (3)$$

This equation establishes the relationship between mean velocity and all fitting parameters for kinesin systems, $\bar{v} = d\frac{(k_f - k_b)k_c}{k_f + k_b + k_c}$, which is used to identify fitting parameters mentioned above and can be determined by experiments [17].

One of the most concerned quantities in our model is the position of the probe $\mathbf{x}_p$. The probe is dragged by a constant hindering force $\mathbf{F}_0$ (to mimic optical tweezers in experiments) and pulled by a molecular motor kinesin via a linear spring with stiffness K. To illustrate the setup, we draw a cartoon in Fig. 1(a), and show the actual simulation system in panel (b) wherein the kinesin and probe are both constrained to move along the $\vec{e}_x$ direction. The movement of the probe is also described by an overdamped Langevin equation

$$\dot{x}_p = \mu_p[K(x_m - x_p) + F_0 + F_{\text{bath}}] + \sqrt{2\mu_p k_B T}\xi_t, \quad (4)$$

where x_p and x_m are the position of the probe and the motor along the $\vec{e}_x$ direction, respectively, μ_p is the mobility of the probe, and $F_{\text{bath}} = -\frac{\partial}{\partial x_p} \sum_i U(|\mathbf{r}_i - \mathbf{x}_p|)$ is the interactions between the probe and bath particles.

For easier comparison with the previous experimental results, in simulations we use SI units and set $k_B T = 4.115$ pN nm for room temperature. Considering that the intracellular environment is dense, and interactions of

various components such as proteins and vesicae are soft, we roughly set the active crowder diameter $R_b = 160$ nm and mobility $\mu_b = 1.0 \times 10^5$ nm/(pN s), set the bath particle density $\rho = N/(L_x L_y L_z) = 1.0/R_b^3$ as a relatively high value, and choose the harmonic potential as the interactions between particles, $U(r) = \frac{\kappa}{2}(\sigma_{pb} - |r|)^2$ for $|r| < \sigma_{pb}$ and $V(r) = \frac{\kappa}{2}(\sigma_{bb} - |r|)^2$ for $|r| < \sigma_{bb}$, where $\sigma_{pb} = (R_p + R_b)/2 = 340$ nm, $\sigma_{bb} = R_b = 160$ nm is the interacting distance of probe-bath particles and bath-bath particles, and κ is the interaction strength which is set as a constant. Other parameters and simulation details are shown in Appendix A. In this work, the main control parameters are the activity of active crowder, measured by Péclet number, which is dimensionless and defined as $\text{Pe} = \frac{\sqrt{D_b/\tau_b}R_b}{\mu_b k_B T}$, where $\sqrt{D_b/\tau_b}$ is the standard deviation of $\mathbf{f}_i$, as well as the persistent time of active crowder τ_b.

Figures 1(d) and 1(e) show several typical simulation trajectories of the kinesin and the probe attached to it. Due to the kinesin walking process, all kinesin/probes move toward the positive x direction. With the constant bath activity and kinetics parameters of kinesin, the influence of hindering load force on kinesin/probe movement is shown in Fig. 1(d). As a matter of course, a larger load force leads to slower movement, as well as a larger distance between the kinesin and probe. Besides, the active fluctuations on the probe contribute significant promotion effect. As shown in Fig. 1(e), with the constant hindering force, larger bath activity induces faster kinesin/probe movement.

Average velocities of probe v for variant bath activities are shown in Figs. 2(a) and 2(c) for a normalized version, and each marker indicates the hindering force F_0 from -2 to -5 pN. Results show that probe velocity v increases with bath activity Pe monotonically in all cases. Especially, normalized velocity $v/v_{\text{Pe}=0}$ shows a stronger enhancement under high hindrance loads. This result is very similar to a most recent *in vitro* experiment [17], wherein the researchers have used optical tweezers to apply a "semitruncated Lévy noise" and an additional constant load force on the probe. They found that motor/probe velocity increases with the magnitude of the noise, and such increases are larger for the stronger load forces. We also investigate the kinesin velocity dependence on persistent time of active bath particles with fixed activity Pe, shown in Fig. 2(e). Simulations show that the probe velocity increases with persistent time τ_b at first and next reaches a plateau. Then, probe velocity weakly decreases at the large τ_b region. To better illustrate these phenomena, velocities depending on various Pe and τ_b have been shown in Fig. 4 in Appendix A.

III. THEORY OF ACTIVE BATH

To understand our simulation results, we propose a mean-field theory method to investigate the system theoretically. The starting point of the theory is the overdamped Langevin equations (1), and the objective of the theory is to obtain an effective movement equation that only contains probe and kinesin variables. To eliminate numerous degrees of freedom of bath particles, we describe the model system at a coarse-grained level, employing an evolution equation for
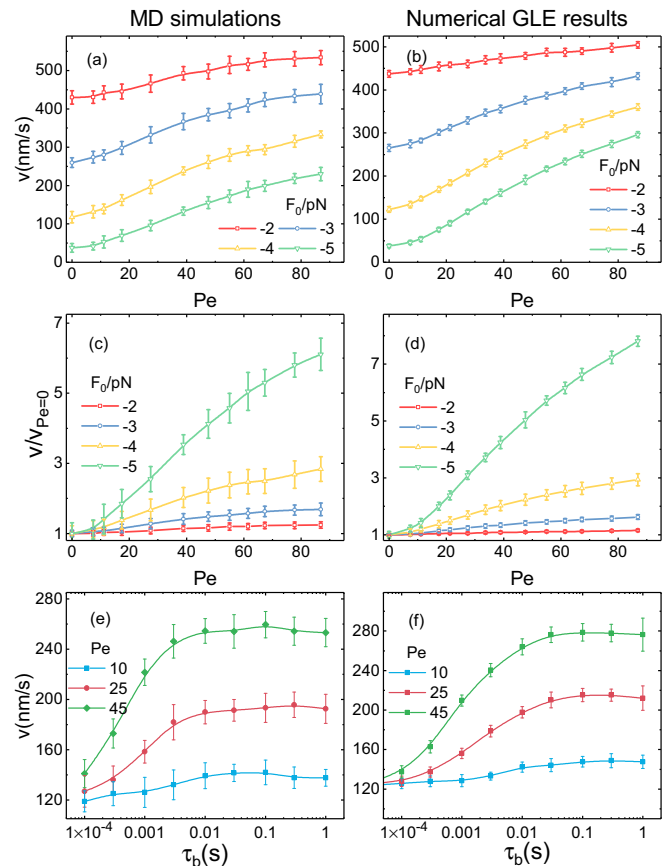

FIG. 2. (a) Simulation results, the average velocity of the probe in the active bath of activity. Each marker indicates various average loads from -2 to -5 pN. (b) Numerical solution of GLE with the same conditions and parameters as (a). (c) and (d): The relative velocity of the probe under the same parameters with (a) and (b), respectively. (e) and (f): Probe velocity for various activity Pe; figures are the plots of v as the function of persistent time τ_b. Other parameters herein: For (a)–(d), we use $\tau_b = 0.01$ s $\approx \frac{R_b^2}{6\mu_b k_B T}$, which is the characteristic rotational time of a Brownian particle with diameter R_b. All figures use $\kappa = 0.003$ pN/nm that indicates a weak interaction; we also test other values of κ, and qualitatively results are not affected by this parameter.

bath particles' density profile $\rho(\mathbf{r}, t)$,

$$\frac{\partial \rho(\mathbf{r}, t)}{\partial t} = \mu_b \nabla_{\mathbf{r}} \cdot \rho(\mathbf{r}, t) \nabla_{\mathbf{r}} \bigg[\int \rho(\mathbf{r}', t) V(|\mathbf{r} - \mathbf{r}'|) d\mathbf{r}'$$

$$+ U(|\mathbf{r} - \mathbf{x_p}|) \bigg] + \nabla \cdot [\sqrt{\rho(\mathbf{r}, t)} \boldsymbol{\xi}^A(\mathbf{r}, t)]$$

$$+ \nabla \cdot [\sqrt{\rho(\mathbf{r}, t)} \boldsymbol{\xi}^T(\mathbf{r}, t)] + \mu_b k_B T \nabla^2 \rho(\mathbf{r}, t), \quad (5)$$

which is a Dean-like equation for active particle system, wherein $\boldsymbol{\xi}^{A,T}(\mathbf{r}, t)$ are noise filed functions. To embody the effect of such a density profile on probe movement, we first solve this equation in Fourier space formally,

$$\frac{\partial \rho_k(t)}{\partial t} \approx -\mu_b k^2 [(k_B T + \rho V_k) \rho_k(t) + \rho U_k e^{i\mathbf{k} \cdot \mathbf{x}_p}]$$

$$+ i\sqrt{\rho} \mathbf{k} \cdot [\tilde{\boldsymbol{\xi}}^T(\mathbf{k}, t) + \tilde{\boldsymbol{\xi}}^A(\mathbf{k}, t)], \quad (6)$$

where ρ is the number density of bath particles, $\tilde{\boldsymbol{\xi}}^{A,T}(\mathbf{k}, t)$, and U_k, V_k are Fourier transforms of noises $\boldsymbol{\xi}^{A,T}(\mathbf{r}, t)$ and potentials $U(r), V(r)$, respectively, with time correlations $\langle \tilde{\xi}_{\alpha}^{A*}(\mathbf{k}, t) \tilde{\xi}_{\beta}^{A}(\mathbf{k}', t') \rangle = \frac{D_b}{\tau_b} \delta_{\alpha\beta}(2\pi)^3 \delta(\mathbf{k} - \mathbf{k}') e^{-|t-t'|/\tau_b}$ and $\langle \tilde{\xi}_{\alpha}^{T*}(\mathbf{k}, t) \tilde{\xi}_{\beta}^{T}(\mathbf{k}', t') \rangle = 2\mu_b k_B T \delta_{\alpha\beta}(2\pi)^3 \delta(\mathbf{k} - \mathbf{k}') \delta(t - t')$. To be clear, Eqs. (5) and (6) are first derived in our Ref. [44], wherein the transport properties of a free tracer particle in the active bath were investigated.

Inserting the formal solution of Eq. (6) into Eq. (4) by utilizing an identity $-\nabla_{\mathbf{x}_p} \sum_i U(|\mathbf{r}_i - \mathbf{x}_p|) \equiv \frac{1}{(2\pi)^3} \int i\mathbf{k} e^{-i\mathbf{k}\cdot\mathbf{x}_p} \rho_k(t) U_k d^3\mathbf{k}$, after a linearized approximation on the memory kernel (see details in Appendix B), we obtain a generalized Langevin equation for the probe

$$\dot{x}_p(t) = -\mu_p \int_{-\infty}^{t} \zeta(t-s)\dot{x}_p(s)ds + \eta_A(t) + \eta_T(t)$$
$$+ \mu_p[K(x_m - x_p) + F_0] + \sqrt{2\mu_p k_B T}\xi_t \quad (7)$$

with memory kernel

$$\zeta(t) = \frac{\mu_p \mu_b \rho}{3(2\pi)^3} \int k^4 U_k^2 a_k e^{-t/a_k} d^3\mathbf{k}, \quad (8)$$

where $a_k = [\mu_b k^2(k_B T + \rho V_k)]^{-1}$ is a characteristic timescale, and $\eta_{A,T}$ are complicated colored noise

$$\eta_{A,T}(t) = \frac{\mu_p\sqrt{\rho}}{(2\pi)^3} \int ik_x U_k$$
$$\times \int_{-\infty}^{t} e^{-(t-s)/a_k} \mathbf{k} \cdot \tilde{\boldsymbol{\xi}}^{A,T}(\mathbf{k}, s)ds d^3\mathbf{k} \quad (9)$$

with time correlation functions

$$\langle \eta_T(t)\eta_T(t') \rangle = \frac{\mu_t^2 \rho \mu_b k_B T}{3(2\pi)^3} \int U_k^2 k^4 a_k e^{-|t-t'|/a_k} d^3\mathbf{k}, \quad (10a)$$

$$\langle \eta_A(t)\eta_A(t') \rangle = \frac{\mu_t^2 \rho D_b}{3(2\pi)^3} \int U_k^2 k^4 \frac{1}{(\tau_b/a_k)^2 - 1}$$
$$\times [\tau_b e^{-|t-t'|/\tau_b} - a_k e^{-|t-t'|/a_k}]d^3\mathbf{k}. \quad (10b)$$

Herein, a generalized fluctuation-dissipation relationship (FDR) is revealed between memory kernel $\zeta(t)$ and noise η_T, and the OU noise of the bath particle brings an explicit violation of the FDR. When the activity of the bath is absent, Eq. (7) reduces to a generalized Langevin equation (GLE) in equilibrium and the FDR holds naturally. Comparing to our Ref. [44], Eqs. (8)–(10) correspond to the situation with adiabatic approximation.

Equations (7)–(9) are the main theoretical results of the present work. They unravel the properties of noise generated by an active environment, and allow us to directly calculate the probe movement and average velocity. Numerical solutions of Eq. (7) are shown in Fig. 2, panels (b), (d), and (f), wherein the parameters are chosen the same as panels (a), (c), and (e), respectively. The numerical algorithm of the generation of noises $\eta_{A,T}$ is shown in Appendix C. Compared with simulation results, the GLE reproduces the acceleration effect of active crowders (a)–(d), quantitatively in most cases. Surprisingly, GLE solutions also show very similar behavior of the relationship between probe velocity and persistent time τ_b, which further confirms the nontrivial phenomenon.
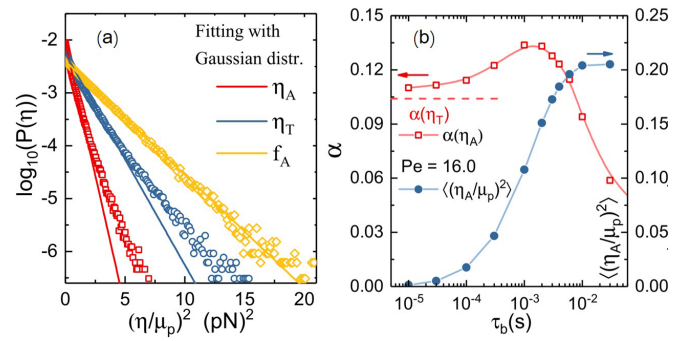

FIG. 3. (a) Distributions for noise η_A (red squares) and η_T (blue round dots); solid lines are fitting lines with hypothetical Gaussian distributions. f$_A$ is an OU process as a reference (yellow diamonds and line), which satisfies an exact Gaussian distribution. Herein, we set $\tau_b = 0.01$ s. (b) Non-Gaussian parameters α for η_A and η_T (red squares and left vertical axis); the formal one depends on persistent τ_b which is drawn here as the horizontal axis. Also, we plot the variance of noise η_A/μ_p (blue points and right vertical axis). Other parameters for all subplots: $\kappa = 0.01$ pN/nm, Pe $= 16.0$.

Theoretical explanations about the mechanism of kinesin acceleration are still in development. In Ref. [17], the authors pointed out that the amplitude of noise is a major factor. Yet in a ratchet potential model [20], not only the noise strength significantly influences the probe dynamics, but also the non-Gaussian property and time correlation behavior of the noise. Herein, with the help of the GLE, it is feasible to investigate which property of the noise dominates kinesin acceleration.

First, we focus on the strength (or amplitude) of the colored noise $\eta_{A,T}(t)$. According to Eq. (9), or more straightforwardly, the time correlation function of $\eta_{A,T}(t)$, the explicit expression for variance,

$$\langle \eta_T^2 \rangle = \frac{\mu_t^2 \rho \mu_b k_B T}{3(2\pi)^3} \int U_k^2 k^4 a_k d^3\mathbf{k}, \quad (11a)$$

$$\langle \eta_A^2 \rangle = \frac{\mu_t^2 \rho D_b}{3(2\pi)^3} \int \frac{U_k^2 k^4 a_k^2}{\tau_b + a_k} d^3\mathbf{k}, \quad (11b)$$

can be obtained, therefore $\langle \eta_A^2 \rangle \propto \text{Pe}^2 \tau_b \int \frac{k^4 U_k^2 a_k^2}{\tau_b + a_k} d^3\mathbf{k}$. As shown in Figs. 2(b) and 2(d), probe velocity v increases with Pe monotonically when τ_b is constant. Although the analytical relation between v and Pe is not given due to the complexity of the memory kernel and colored noise, qualitatively variance of noise η_A definitely makes a positive contribution to kinesin acceleration.

Another quantity we are concerned about is the non-Gaussian property of these two colored noises. To intuitively show the distributions of such noises, we plot the probability distribution function $P(\eta)$ in Fig. 3(a). The red square and blue round hollow dots represent η_A and η_T, respectively, and solid curves are their Gaussian fitting. Interestingly, both η_T and η_A show heavy tail distributions and clearly deviate from Gaussian distributions. As a contrast, the distribution function of OU noise f$_A$ is also plotted with yellow diamond dots, which perfectly satisfies the Gaussian distribution. Noticing that Lévy noise also has such heavy tail distribution [17], as well as the ECP noise [20], they all have a nontrivial acceleration effect on kinesin. To quantitatively investigate

this property, we then calculate the non-Gaussian parameter $\alpha(\eta) = \frac{\langle\eta^4\rangle}{3\langle\eta^2\rangle^2} - 1$ of $\eta_{A,T}(t)$. These quantities are not functions of temperature T or activity Pe, and therefore the contribution of non-Gaussian properties cannot be seen in Figs. 2(a)–2(d). Yet $\alpha(\eta_A)$ is a function of τ_b, and both simulation and GLE solution show the same dependency relationship of kinesin velocity on τ_b. Hence we plot the non-Gaussian parameter α (red squares, left axis) and corresponding noise variance (blue dots, right axis) as functions of persistent time τ_b in Fig. 3(b). When $\tau_p \to 0$, η_A reduces to the noise η_T [under an effective temperature $T_{\text{eff}} = D_b/(\mu_b k_B)$], and its non-Gaussian parameter is shown as a red horizontal dashed line in Fig. 3(b). As τ_b increases, $\langle\eta_A^2\rangle$ monotonically increases and then reaches a plateau, which is very similar to the velocity increase with τ_b at short and intermediate regions. As shown in Figs. 2(e) and 2(f), when τ_b is large enough, the kinesin velocity slightly decreases with τ_b. This weak decrease in behavior has not been seen in the noise variance. On the contrary, a strongly nonmonotonic dependence of $\alpha(\eta_A)$ on τ_b is observed. The non-Gaussian parameter $\alpha(\eta_A)$ rapidly decreases with τ_b when it is large. This phenomenon is very likely to lead to a weak decrease in the kinesin velocity. In general, variance indeed makes the major contribution to the kinesin acceleration, while the non-Gaussian property also makes a minor yet positive contribution to it.

IV. CONCLUSION

In summary, we have proposed a bottom-up model consisting of a Markov model for kinesin and a mean-field model of active particle bath, to investigate the acceleration behavior of kinesin and probe attached to it in complex intracellular environment. Simulations show kinesin velocity increases with bath activity monotonically, especially for larger load situations where more significant acceleration effect is observed. We also establish a coarse-grained theoretical framework to describe the active bath and obtain a generalized Langevin equation for probe movement. The effects of active bath on the probe are simplified into a memory kernel and two effective noises. Numerical calculations of the GLE show very good agreement with simulation data. Furthermore, the introduction of the theory allows us to study the noise property conveniently and to investigate which one of them is the essential to kinesin acceleration. Comparing simulations and numerical solutions for GLE, we find out that the variance of noise plays a major role in kinesin acceleration, while non-Gaussian property brings positive yet minor contributions.

Our model and theory bring a quantifiable research approach to active fluctuations in living cells, which bridges between phenomenological description of kinesin movement and underlying principles of statistical physics. For further study, with more information input such as accurate interacting parameters, we believe our model could give more accurate results, and deeper understanding on the noise property. In addition, the theory of active bath is independent of the kinesin model, which also serves as a way to investigate the active environment, the generality of which could lead to numerous other applications in other probe-bath interacting systems.

APPENDIX A: NUMERICAL SIMULATIONS

Numerical simulations are run in a three-dimensional box $(L_x, L_y, L_z) = (40\sigma, 10\sigma, 10\sigma)$ with periodic boundary, where $\sigma = 160$ nm is the unit of length. In the present coarse-grained model, both the kinesin and the probe movements are constrained on a fixed line $(y, z) = (L_y/2, L_z/2)$. The volume repulsive interactions are only considered between bath-bath particles and bath-probe, meaning that the kinesin's volume repulsive interaction is not considered. The diameter of bath particle and the probe are set as $R_b = \sigma$, $R_p = 3.25\sigma$, so that interparticle distance $\sigma_{pb} = 2.125\sigma$. The temperature is set as the room temperature, and therefore $k_B T = 4.115$ pN nm, which is used as the unit of the energy. The mobility of the bath particle is $\mu_b = 1.0 \times 10^5$ nm/(pN s), which can be used to label the unit of time $\tau_u = \sigma^2/(\mu_b k_B T) = 6.22 \times 10^{-2}$ s. We set the probe diameter $R_p = 520$ nm and mobility $\mu_p = 0.308 \times 10^5$ nm/(pN s).
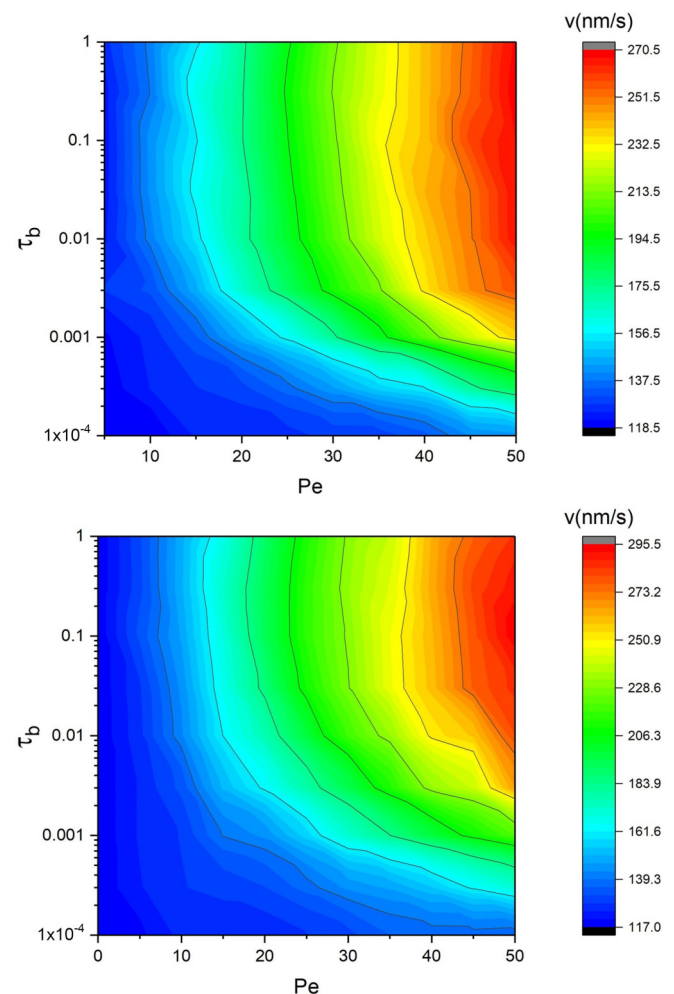

FIG. 4. Probe velocity for various activity Pe and τ_b. The upper figure is the result of direct simulations, and the lower one is the numerical result of GLE.

In simulations, we use the time step $\delta t = 5.0 \times 10^{-6}$ s (to keep $k_{c,b,f}\delta t \ll 1$, $\delta_t \ll \tau_b$, and $\delta t \ll \tau_u$). For each time interval, both the Markov dynamics for kinesin and the Langevin dynamics for probe and bath particles are performed. For each simulation, the system is allowed to reach a steady state over $10^6\delta t$, and then the kinesin/probe's displacements and velocities are averaged over the following $10^7\delta t$ time interval. The variance of the velocity is calculated by simulations of at least 20 times with the exact same parameters and different random number seeds. We find that more average counts did not have a significant effect on the reduction of the variance.

For the numerical calculation of the generalized Langevin equation (GLE), the time step is also set as $\delta t = 5.0 \times 10^{-6}$ s. The generation of the complex color noises is shown in Appendix C. Velocities and their variances are calculated by over 10^7 time steps and 50 trajectories.

The Markov transition migrates from Ref. [17], and parameters in the main text Eqs. (2) and (3) also come from this reference: $k_f^0 = 1002$ s^{-1}, $k_b^0 = 27.9$ s^{-1}, $k_c = 102$ s^{-1}, $d_f = 3.61$ nm, $d_b = 1.14$ nm.

To better illustrate Figs. 2(e) and 2(f) in the main text, we plot the probe velocity dependence on Pe and persistent time τ_b, as shown in Fig. 4.

APPENDIX B: DEAN'S EQUATION FOR ACTIVE BATH AND EFFECTIVE GENERALIZED LANGEVIN EQUATION FOR PROBE

This section gives the derivation details of Eq. (4) in the main text. To be clear, this derivation shares the same idea as our Ref. [44]. For clarity and the convenience of reading, we arrange this part here and rewrite something since only adiabatic is used in the current work.

The starting point is the Langevin equation for bath particles,

$$
\dot{\mathbf{r}}_i = -\mu_b \nabla_i \left[\sum_{j \neq i} V(|\mathbf{r}_i - \mathbf{r}_j|) + U(|\mathbf{r}_i - \mathbf{x}_p|) \right]
$$

$$
+ \mathbf{f}_i + \sqrt{2\mu_b k_B T} \boldsymbol{\xi}_i, \tag{B1a}
$$

$$
\tau_b \dot{\mathbf{f}}_i = -\mathbf{f}_i + \sqrt{2D_b} \boldsymbol{\eta}_i. \tag{B1b}
$$

Introducing the single-particle density $\rho_i(\mathbf{r}, t) = \delta(\mathbf{r} - \mathbf{r}_i(t))$ and the collective one $\rho(\mathbf{r}, t) = \sum_{i=1}^{N} \rho_i(\mathbf{r}, t)$, for an arbitrary function of bath particle coordinate $g(\mathbf{r}_i)$ with natural boundary condition, according to the Itō calculus, one has

$$
\frac{dg(\mathbf{r}_i)}{dt} = \left\{ -\mu_b \nabla_i \left[\sum_{j \neq i} V(|\mathbf{r}_i - \mathbf{r}_j|) + U(|\mathbf{r}_i - \mathbf{x_p}|) \right] + \mathbf{f}_i + \sqrt{2\mu_b k_B T} \boldsymbol{\xi}_i \right\} \cdot \nabla_i g(\mathbf{r}_i)
$$

$$
+ \mu_b k_B T \nabla_i^2 g(\mathbf{r}_i)
$$

$$
= \int \rho_i(\mathbf{r}, t) \left\{ \left(-\mu_b \nabla_\mathbf{r} \left[\sum_{j \neq i} V(|\mathbf{r} - \mathbf{r}_j|) + U(|\mathbf{r} - \mathbf{x_p}|) \right] + \mathbf{f}_i + \sqrt{2\mu_b k_B T} \boldsymbol{\xi}_i \right) \cdot \nabla_\mathbf{r} g(\mathbf{r}) \right.
$$

$$
+ \mu_b k_B T \nabla_\mathbf{r}^2 g(\mathbf{r}) \Big\} d\mathbf{r}
$$

$$
= \int \rho_i(\mathbf{r}, t) \left\{ \left(-\mu_b \nabla_\mathbf{r} \left[\int \rho(\mathbf{r}', t) V(|\mathbf{r} - \mathbf{r}'|) d\mathbf{r}' + U(|\mathbf{r} - \mathbf{x_p}|) \right] + \mathbf{f}_i + \sqrt{2\mu_b k_B T} \boldsymbol{\xi}_i \right) \cdot \nabla_\mathbf{r} g(\mathbf{r}) \right.
$$

$$
+ \mu_b k_B T \nabla_\mathbf{r}^2 g(\mathbf{r}) \Big\} d\mathbf{r}
$$

$$
= \int g(\mathbf{r}) \left\{ \nabla_\mathbf{r} \cdot \left(\mu_b \nabla_\mathbf{r} \left[\int \rho(\mathbf{r}', t) V(|\mathbf{r} - \mathbf{r}'|) d\mathbf{r}' + U(|\mathbf{r} - \mathbf{x_p}|) \right] - \mathbf{f}_i - \sqrt{2\mu_b k_B T} \boldsymbol{\xi}_i \right) \rho_i(\mathbf{r}, t) \right.
$$

$$
+ \mu_b k_B T \nabla_\mathbf{r}^2 \rho_i(\mathbf{r}, t) \Big\}. \tag{B2}
$$

In the third step, it seems there is an extra term $V(0)$, but it vanishes due to the $\nabla_\mathbf{r}$ operator, and the last step used part integral. On the other hand, with the identity $\frac{d}{dt} g(\mathbf{r}_i) = \frac{d}{dt} \int \rho_i(\mathbf{r}, t) g(\mathbf{r}) d\mathbf{r} = \int \frac{\partial \rho_i(\mathbf{r},t)}{\partial t} g(\mathbf{r}) d\mathbf{r}$, and considering the arbitrariness of function $g(\mathbf{r})$, immediately

$$
\frac{\partial \rho_i(\mathbf{r}, t)}{\partial t} = \nabla_\mathbf{r} \cdot \rho_i(\mathbf{r}, t) \left[\mu_b \nabla_\mathbf{r} \left(\int \rho(\mathbf{r}', t) V(|\mathbf{r} - \mathbf{r}'|) d\mathbf{r}' + U(|\mathbf{r} - \mathbf{x_p}|) \right) - \mathbf{f}_i - \sqrt{2\mu_b k_B T} \boldsymbol{\xi}_i \right]
$$

$$
+ \mu_b k_B T \nabla_\mathbf{r}^2 \rho_i(\mathbf{r}, t) \tag{B3}
$$

then the collective density function

$$\frac{\partial \rho(\mathbf{r}, t)}{\partial t} = \mu_b \nabla \cdot \left[\rho(\mathbf{r}, t) \nabla \left(\int \rho(\mathbf{r}', t) V(|\mathbf{r} - \mathbf{r}'|) + U(|\mathbf{r} - \mathbf{x}_p|) \right) \right]$$
$$+ \sum_i [-\nabla \cdot (\mathbf{f}_i \rho_i) - \sqrt{2\mu_b k_B T} \nabla \cdot (\rho_i \boldsymbol{\xi}_i)] + \mu_b k_B T \nabla^2 \rho(\mathbf{r}, t). \tag{B4}$$

This equation is not self-consistent yet, since $\mathbf{f}_i \rho_i$ and $\rho_i \boldsymbol{\xi}_i$ terms still exist. To fix this, following Dean's method [53], we introduce two noise fields $\chi_{1,2}(\mathbf{r}, t)$ as functions of $\rho(\mathbf{r}, t)$ to replace $\chi_1'(\mathbf{r}, t) = -\sum_i \nabla \cdot (\mathbf{f}_i \rho_i)$ and $\chi_2'(\mathbf{r}, t) = -\sqrt{2\mu_b k_B T} \sum_i \nabla \cdot (\rho_i \boldsymbol{\xi}_i)$. Considering

$$\langle \chi_1'(\mathbf{r}, t) \chi_1'(\mathbf{r}', t') \rangle = \frac{D_b}{\tau_b} e^{-|t-t'|/\tau_b} \sum_i \nabla \cdot \nabla'[\rho_i(\mathbf{r}, t)\rho_i(\mathbf{r}', t')]$$
$$= \frac{D_b}{\tau_b} e^{-|t-t'|/\tau_b} \nabla \cdot \nabla'[\rho(\mathbf{r}, t)\delta(\mathbf{r} - \mathbf{r}')], \tag{B5a}$$

$$\langle \chi_2'(\mathbf{r}, t) \chi_2'(\mathbf{r}', t') \rangle = 2\mu_b k_B T \delta(t - t') \sum_i \nabla \cdot \nabla'[\rho_i(\mathbf{r}, t)\rho_i(\mathbf{r}', t')]$$
$$= 2\mu_b k_B T \delta(t - t') \nabla \cdot \nabla'[\rho(\mathbf{r}, t)\delta(\mathbf{r} - \mathbf{r}')], \tag{B5b}$$

we construct noise field $\chi_1(\mathbf{r}, t) = \nabla \cdot [\sqrt{\rho(\mathbf{r}, t)} \boldsymbol{\xi}^A(\mathbf{r}, t)]$ and $\chi_2(\mathbf{r}, t) = \nabla \cdot [\sqrt{\rho(\mathbf{r}, t)} \boldsymbol{\xi}^T(\mathbf{r}, t)]$ to keep the correlations of χ_1 and χ_1', χ_2 and χ_2' equal, where $\boldsymbol{\xi}^{A,T}(\mathbf{r}, t)$ are also noise field with correlation $\langle \boldsymbol{\xi}^A(\mathbf{r}, t) \boldsymbol{\xi}^A(\mathbf{r}', t') \rangle = \frac{D_b}{\tau} e^{-|t-t'|/\tau_b} \delta(\mathbf{r} - \mathbf{r}')\mathbf{I}$ and $\langle \boldsymbol{\xi}^T(\mathbf{r}, t) \boldsymbol{\xi}^T(\mathbf{r}', t') \rangle = 2\mu_b k_B T \delta(-|t - t'|)\delta(\mathbf{r} - \mathbf{r}')\mathbf{I}$, respectively. Now we achieve a self-consistent equation for the evolution of $\rho(\mathbf{r}, t)$,

$$\frac{\partial \rho(\mathbf{r}, t)}{\partial t} = \mu_b \nabla_{\mathbf{r}} \cdot \rho(\mathbf{r}, t) \nabla_{\mathbf{r}} \left[\int \rho(\mathbf{r}', t) V(|\mathbf{r} - \mathbf{r}'|) d\mathbf{r}' + U(|\mathbf{r} - \mathbf{x_p}|) \right]$$
$$+ \mu_b k_B T \nabla^2 \rho(\mathbf{r}, t) + \nabla \cdot [\sqrt{\rho(\mathbf{r}, t)} \boldsymbol{\xi}^A(\mathbf{r}, t)] + \nabla \cdot [\sqrt{\rho(\mathbf{r}, t)} \boldsymbol{\xi}^T(\mathbf{r}, t)]. \tag{B6}$$

This equation is one of the central results in this section, also known as Dean's equation.

To eliminate variables of bath particle positions, we use a mean-field theory to describe the active bath. Using Eq. (B6) and assuming the environment is isotropic, homogeneous, and has no special structures (suitable for weak interaction and dense situations), the evolution equation for bath density can be simplified as

$$\frac{\partial \rho_k(t)}{\partial t} \approx -\mu_b k^2 [(k_B T + \rho V_k)\rho_k(t) + \rho U_k e^{i\mathbf{k} \cdot \mathbf{x}_p}] + i\sqrt{\rho} \mathbf{k} \cdot [\tilde{\boldsymbol{\xi}}^T(\mathbf{k}, t) + \tilde{\boldsymbol{\xi}}^A(\mathbf{k}, t)] \tag{B7}$$

in Fourier space, where $\rho_k(t)$, U_k, V_k, $\tilde{\boldsymbol{\xi}}^A(\mathbf{k}, t)$, and $\tilde{\boldsymbol{\xi}}^T(\mathbf{k}, t)$ are Fourier transforms of $\rho(\mathbf{r}, t)$, $U(r)$, $V(r)$, $\boldsymbol{\xi}^A(\mathbf{r}, t)$, and $\boldsymbol{\xi}^T(\mathbf{r}, t)$, respectively. This equation has a formal solution

$$\rho_k(t) = \int_{-\infty}^{t} e^{-(t-s)/a_k} \{-\mu_b k_B T k^2 \rho U_k e^{i\mathbf{k} \cdot \mathbf{x}_p} + i\sqrt{\rho} \mathbf{k} \cdot [\tilde{\boldsymbol{\xi}}^A(\mathbf{k}, s) + \tilde{\boldsymbol{\xi}}^T(\mathbf{k}, s)]\} ds, \tag{B8}$$

where $a_k = [\mu_b k^2 (k_B T + \rho V_k)]^{-1}$. Using the identity (performing the Fourier transition and its inverse transform on the left-hand side)

$$-\nabla_{\mathbf{x}_p} \sum_i U(|\mathbf{r}_i - \mathbf{x}_p|) \equiv \frac{1}{(2\pi)^3} \int i\mathbf{k} e^{-i\mathbf{k} \cdot \mathbf{x}_p} \rho_k(t) U_k d^3 \mathbf{k}, \tag{B9}$$

and inserting the formal solution (B8) into the Langevin equation for probe Eq. (1) in the main text, we get a generalized Langevin equation for probe movement along the $\vec{e}_x$ direction,

$$\dot{x}_p = \mu_p \int_{-\infty}^{t} \tilde{F}(t - s) ds + \mu_p [K(x_m - x_p) + F_0] + \eta_A(x_p(t), t) + \eta_T(x_p(t), t) + \sqrt{2\mu_p k_B T} \xi_t, \tag{B10}$$

where $\tilde{F}(t) = -\frac{\mu_b \rho}{(2\pi)^3} \int i k_x k^2 U_k^2 e^{-ik_x[x_p(t) - x_p(s)]} e^{-(t-s)/a_k}$ is a complex memory kernel, and

$$\eta_{A,T}(x_p(t), t) = \frac{\mu_p \sqrt{\rho}}{(2\pi)^3} \int i k_x U_k e^{-ik_x x_p(t)} \int_{-\infty}^{t} e^{-(t-s)/a_k} \mathbf{k} \cdot \tilde{\boldsymbol{\xi}}^{A,T}(\mathbf{k}, s) ds d^3 \mathbf{k} \tag{B11}$$

is the colored noise term induced by the bath. This memory kernel is very complex to use, yet to the linear order, the memory kernel can be simplified to the form $\mu_p \int_{-\infty}^{t} \tilde{F}(t - s) ds \approx -\int_{-\infty}^{t} \zeta(t - s)\dot{x}_p(s) ds$, where

$$\zeta(t) = \frac{\mu_p \mu_b \rho}{3(2\pi)^3} \int k^4 U_k^2 a_k e^{-t/a_k} d^3 \mathbf{k}, \tag{B12}$$

which is much easier to employ. As for the noise $\eta_{A,T}(x_p(t), t)$, considering that the timescale of probe movement is much slower than bath particles, we use the adiabatic approximation so that the noises can be simplified into

$$\eta_{A,T}(t) = \frac{\mu_p \sqrt{\rho}}{(2\pi)^3} \int ik_x U_k \int_{-\infty}^{t} e^{-(t-s)/a_k} \mathbf{k} \cdot \tilde{\boldsymbol{\xi}}^{A,T}(\mathbf{k}, s) ds d^3\mathbf{k} \tag{B13}$$

with time correlations

$$\langle \eta_T(t)\eta_T(t')\rangle = \frac{2\mu_t^2 \rho \mu_b k_B T}{(2\pi)^3} \int k_x^2 U_k^2 k^2 \frac{a_k}{2} e^{-|t-t'|/a_k} d^3\mathbf{k}, \tag{B14a}$$

$$\langle \eta_A(t)\eta_A(t')\rangle = \frac{\mu_t^2 \rho D_b}{(2\pi)^3} \int k_x^2 U_k^2 k^2 \frac{1}{(\tau_b/a_k)^2 - 1} [\tau_b e^{-|t-t'|/\tau_b} - a_k e^{-|t-t'|/a_k}] d^3\mathbf{k}. \tag{B14b}$$

APPENDIX C: GENERATION OF COMPLEX COLORED NOISE

According to Eq. (B13), and using the Greek alphabet to express the vector component, $\eta_{A,T}$ in the α component is

$$\eta_{A,T}^{\alpha}(t) = \frac{\mu_t \sqrt{\rho}}{(2\pi)^3} \int d^3\mathbf{k} k^\alpha e^{-i\mathbf{k}\cdot\mathbf{x}_p(t)} U_k \int_{-\infty}^{t} e^{-(t-s)/a_k} \left[\sum_\beta k^\beta \tilde{\xi}_\beta^{A,T}(\mathbf{k}, s) \right] ds. \tag{C1}$$

Since $\tilde{\xi}_\beta^{A,T}(\mathbf{k}, t) = \int \xi_\beta^{A,T}(\mathbf{r}, t) e^{i\mathbf{k}\cdot\mathbf{r}} d^3\mathbf{r}$, as well as the correlations shown in Appendix B, one has

$$\langle \tilde{\xi}_\alpha^{A*}(\mathbf{k}, t)\tilde{\xi}_\beta^{A}(\mathbf{k}', t')\rangle = \frac{D_b}{\tau_b} \delta_{\alpha\beta}(2\pi)^3 \delta(\mathbf{k} - \mathbf{k}') e^{-|t-t'|/\tau_b}, \tag{C2a}$$

$$\langle \tilde{\xi}_\alpha^{T*}(\mathbf{k}, t)\tilde{\xi}_\beta^{T}(\mathbf{k}', t')\rangle = 2\mu_b k_B T \delta_{\alpha\beta}(2\pi)^3 \delta(\mathbf{k} - \mathbf{k}')\delta(t - t'). \tag{C2b}$$

Therefore random variables $\tilde{\xi}_\alpha^{A,T}(\mathbf{k}, t)$ can be divided into two independent stochastic processes in time and k space,

$$\tilde{\xi}_\alpha^{A}(\mathbf{k}, t) dt d^3\mathbf{k} = \sqrt{\frac{D_b}{\tau_b}} (2\pi)^{3/2} f_\alpha(t) dt d^3W_{\mathbf{k}}, \tag{C3a}$$

$$\tilde{\xi}_\alpha^{T}(\mathbf{k}, t) dt d^3\mathbf{k} = \sqrt{2\mu_b k_B T} (2\pi)^{3/2} dW_t d^3W_{\mathbf{k}}, \tag{C3b}$$

where W_t and $W_{\mathbf{k}}$ are independent Wiener processes, $f_\alpha(t)$ is an dimensionless OU process with $\tau_b \dot{f}_\alpha(t) = -f_\alpha(t) + \sqrt{2\tau_b}\xi_t$ (ξ_t stands for standard white noise), formal solution $f_\alpha(t) = \sqrt{\frac{2}{\tau_b}} \int_{-\infty}^{t} e^{-(t-s)/\tau_b}\xi_s ds$, and time correlation $\langle f_\alpha(t)f_\beta(t')\rangle = \delta_{\alpha\beta} e^{-|t-t'|/\tau_b}$.

This proposal indicates Eq. (C1) can be rewritten as

$$\eta_A^{\alpha}(t) = -\frac{\mu_t}{(2\pi)^{3/2}} \sqrt{\rho D_b} \int k_\alpha e^{-i\mathbf{k}\cdot\mathbf{x}(t)} U_k \sum_\beta k_\beta B_\beta^A(\mathbf{k}, t) d^3W_{\mathbf{k}}$$

$$= -\frac{\mu_t}{d(2\pi)^{3/2}} \sqrt{\rho D_b} \int k^2 e^{-i\mathbf{k}\cdot\mathbf{x}(t)} U_k B_\alpha^A(\mathbf{k}, t) d^3W_{\mathbf{k}}, \tag{C4a}$$

$$\eta_T^{\alpha}(t) = -\frac{\mu_t}{(2\pi)^{3/2}} \sqrt{2\rho \mu_b k_B T} \int k_\alpha e^{-i\mathbf{k}\cdot\mathbf{x}(t)} U_k \sum_\beta k_\beta B_\beta^T(\mathbf{k}, t) d^3W_{\mathbf{k}}$$

$$= -\frac{\mu_t}{d(2\pi)^{3/2}} \sqrt{2\rho \mu_b k_B T} \int k^2 e^{-i\mathbf{k}\cdot\mathbf{x}(t)} U_k B_\alpha^T(\mathbf{k}, t) d^3W_{\mathbf{k}}, \tag{C4b}$$

where $B_\alpha^A(\mathbf{k}, t) = \int_{-\infty}^{t} \tau_b^{-1/2} e^{-(t-s)/a_k} f_\alpha(s) ds$, $B_\alpha^T(\mathbf{k}, t) = \int_{-\infty}^{t} e^{-(t-s)/a_k} dW_s$ are independent stochastic processes which can be generated numerically.

In detail, one has $\dot{B}_\alpha^T = -a_k^{-1} B_\alpha^T + \xi_t$, which is also an OU process with $\langle B_\alpha^T(t)B_\alpha^T(t')\rangle = \frac{a_k}{2} e^{-|t-t'|/a_k}$. Therefore the initial value of $B_\alpha^T(\mathbf{k}, t)$ can be set as a Gaussian random number with zero mean and variance $a_k/2$. Numerically, $B_\alpha^T(\mathbf{k}, t_{i+1}) = e^{-\Delta t/a_k} B_\alpha^T(\mathbf{k}, t_i) + \sqrt{\frac{a_k}{2}(1 - e^{-2\Delta t/a_k})} u_{i+1}$, where $\Delta t = t_{i+1} - t_i$ is the time interval, and $\{u_i\}$ is a set of independent Gaussian random variables of zero mean and variance 1. Here we emphasize that the ordinary Euler-Maruyama algorithm [i.e., $B_\alpha^T(\mathbf{k}, t_{i+1}) = (1 - \Delta t/a_k)B_\alpha^T(\mathbf{k}, t_i) + \sqrt{\Delta t} u_i$] is not suitable for the present case, since the characteristic timescale a_k is dependent on $k = |\mathbf{k}|$ and it is not practical to choose a small enough interval such that $\Delta t \ll a_k$ for all k's.

On the other hand, $\dot{B}_\alpha^A = -a_k^{-1} B_\alpha^A + \tau_b^{-1/2} f_\alpha(t)$ and $\ddot{B}_\alpha^A + (a_k^{-1} + \tau_b^{-1})\dot{B}_\alpha^A + (a_k\tau_b)^{-1}B_\alpha^A = \frac{\sqrt{2}}{\tau_b}\xi_t$ leads to the solution

$$B_\alpha^A(\mathbf{k}, t) = \frac{a_k \sqrt{2}}{\tau_b - a_k} \int_{-\infty}^{t} [e^{-(t-s)/\tau_b} - e^{-(t-s)/a_k}] dW_s \tag{C5}$$

with correlation function $\langle B_\alpha^A(t)B_\alpha^A(t')\rangle = \frac{1}{(\tau_b/a_k)^2-1}[\tau_b e^{-|t-t'|/\tau_b} - a_k e^{-|t-t'|/a_k}]$. So the initial value of $B_\alpha^A(t)$ can be a set of Gaussian random numbers with zero mean and variance $\frac{a_k^2}{\tau_b+a_k}$. Consequently, $B_\alpha^A(\mathbf{k},t)$ can be written as

$$B_\alpha^A(\mathbf{k},t_{i+1}) = e^{-\Delta t/a_k}B_\alpha^A(\mathbf{k},t_i) + \frac{a_k\sqrt{2}}{\tau_b - a_k}\left[(e^{-\Delta t/\tau_b} - e^{-\Delta t/a_k})\sqrt{\frac{\tau_b}{2}}f_\alpha(t_i) + G_\alpha(\mathbf{k},t_i)\right], \tag{C6}$$

where $G_\alpha(\mathbf{k},t_i) = \int_{t_i}^{t_{i+1}}[e^{-(t_{i+1}-s)/\tau_b} - e^{-(t_{i+1}-s)/a_k}]dW_s$, with expectation

$$\langle G_\alpha(\mathbf{k},t_i)G_\alpha(\mathbf{k},t_j)\rangle = \delta_{ij}\left[\frac{\tau_b}{2}(1 - e^{-2\Delta t/\tau_b}) + \frac{a_k}{2}(1 - e^{-2\Delta t/a_k}) - \frac{2\tau_b a_k}{a_k + \tau_b}(1 - e^{-\Delta t/\tau_b}e^{-\Delta t/a_k})\right]$$
$$\equiv \delta_{ij}\mathcal{G}_\alpha(\mathbf{k},\Delta t), \tag{C7}$$

which is of order $\frac{\Delta t^3(a_k-\tau_b)^2}{3a_k^2\tau_b^2} + O(\Delta t^4)$. Finally, the exact numerical algorithm to generate $B_\alpha^A(\mathbf{k},t_i)$ is

$$B_\alpha^A(\mathbf{k},t_{i+1}) = e^{-\Delta t/a_k}B_\alpha^A(\mathbf{k},t_i) + \frac{a_k\sqrt{2}}{\tau_b - a_k}\left[(e^{-\Delta t/\tau_b} - e^{\Delta t/a_k})\sqrt{\frac{\tau_b}{2}}f_\alpha(t_i) + \sqrt{\mathcal{G}_\alpha(\mathbf{k},\Delta t)}v_i\right], \tag{C8a}$$

$$f_\alpha(t_{i+1}) = e^{-\Delta t/\tau_b}f_\alpha(t_i) + \sqrt{1 - e^{-2\Delta t/\tau_b}}w_i, \tag{C8b}$$

where $\{v_i\}$ and $\{w_i\}$ are sets of independent Gaussian random variables of zero mean and variance 1. Comparing with the direct differential algorithm $B_\alpha^A(t_{i+1}) = (1 - \Delta t/a_k)B_\alpha^A(t_i) + \tau_b^{-1/2}f_\alpha(t)\Delta t$, our method is suitable for the situation when $\Delta t \geqslant a_k$.

For the 3d system, the stochastic integral over $d^3W_{\mathbf{k}}$ can be simplified through the following method. For simplicity, consider an arbitrary bounded stochastic integral $\eta = \iiint f(\mathbf{k})d^3W_{\mathbf{k}}$ with $f(\mathbf{k}) = f(k)$, $k = |\mathbf{k}|$. One has $\langle\eta\rangle = 0$ and $\langle\eta^2\rangle = \iiint f^2(k)d^3\mathbf{k} = 4\pi\int_0^\infty f^2(k)k^2dk$. Now consider another one-dimensional integral $\varphi = a\int_0^\infty f(k)k^b dW_k$; one also has $\langle\varphi^2\rangle = a^2\int_0^\infty f^2(k)k^{2b}dk$. Let $\langle\eta^2\rangle = \langle\varphi^2\rangle$; immediately one gets $a = \sqrt{4\pi}$ and $b = 1$. This method can greatly simplify the calculation of $\eta_{A,T}^\alpha(\mathbf{x},t)$.

At last, under the adiabatic approximation, we have

$$\eta_T^\alpha(0,t) = -\frac{\mu_t}{3(2\pi)^{3/2}}\sqrt{8\pi\rho\mu_b k_B T}\int_0^\infty k^3 U_k B_\alpha^T(k,t)dW_k, \tag{C9a}$$

$$\eta_A^\alpha(0,t) = -\frac{\mu_t}{3(2\pi)^{3/2}}\sqrt{4\pi\rho D_b}\int_0^\infty k^3 U_k B_\alpha^A(k,t)dW_k. \tag{C9b}$$

Now we consider the asymptotic behavior of the correlation function at a large timescale. In this situation, only very small k's contribute to the integral. Therefore one may assume $e^{-|t-t'|/a_k} \approx e^{-|t-t'|\mu_b k^2(k_B T+\rho V_0)}$, where V_0 notes for $V(\mathbf{k}=0)$. Consequently, for η_T, one has

$$\langle\eta_T^\alpha(0,t)\eta_T^\alpha(0,t')\rangle \approx \frac{\mu_t^2\rho\mu_b k_B T}{(2\pi)^d}\int\frac{k_\alpha^2 U_0^2}{\mu_b(k_B T + \rho V_0)}e^{-|t-t'|\mu_b(k_B T+\rho V_0)k^2}d^3\mathbf{k}$$
$$= \frac{\mu_t^2\rho}{(2\pi)^d(1 + \rho V_0/k_B T)}\frac{1}{2p}\left(\frac{\pi}{p}\right)^{\frac{d}{2}}, \tag{C10}$$

where U_0 also stands for $U(\mathbf{k}=0)$, $p = |t-t'|\mu_b(k_B T + \rho V_0)$. As a result, we get $\langle\eta_T^\alpha(0,t)\eta_T^\alpha(0,t')\rangle \propto |t-t'|^{-(d/2+1)}$.

For η_A, the exponential decay part $e^{-|t-t'|/\tau_b}$ has no contribution to the long-time decay behavior anyway. One may only consider the other part, i.e.,

$$\langle\eta_A^\alpha(0,t)\eta_A^\alpha(0,t')\rangle \asymp \frac{\mu_t^2\rho D_b}{(2\pi)^2}\int k_\alpha^2 U_k^2\frac{k^2 a_k}{1 - (\tau_b/a_k)^2}e^{-|t-t'|/a_k}d^3\mathbf{k}$$
$$\approx \frac{\mu_t^2\rho}{(2\pi)^d}\frac{D_b}{\mu_b(k_B T + \rho V_0)}\int\frac{k_\alpha^2 U_0^2}{1 - [\mu_b(k_B T + \rho V_0)\tau_b]^2 k^4}e^{-|t-t'|\mu_b(k_B T+\rho V_0)k^2}d^3\mathbf{k}$$
$$\approx \frac{\mu_t^2\rho}{(2\pi)^d}\frac{D_b}{\mu_b(k_B T + \rho V_0)}\frac{1}{2p}\left(\frac{\pi}{p}\right)^{\frac{d}{2}}. \tag{C11}$$

Clearly the long-time behavior also follows a power law $\langle\eta_A^\alpha(0,t)\eta_A^\alpha(0,t')\rangle \propto |t-t'|^{-(d/2+1)}$.

Another situation is the weak interaction limit between bath particles, $k_B T \gg \rho V(k)$, then $a_k \approx [\mu_b k^2 k_B T]^{-1}$. Herein the correlation of η_T is

$$
\begin{aligned}
\langle \eta_T^\alpha(0, t) \eta_T^\alpha(0, t') \rangle &\approx \frac{\mu_t^2 \rho \mu_b k_B T}{(2\pi)^d} \int \frac{k_\alpha^2 \iint e^{i\mathbf{k} \cdot (\mathbf{r} + \mathbf{r}')} U(r) U(r') d\mathbf{r} d\mathbf{r}'}{\mu_b k_B T} e^{-|t-t'|\mu_b k_B T k^2} d^3 \mathbf{k} \\
&= \frac{\mu_t^2 \rho}{(2\pi)^2} \int k_\alpha^2 \iint U(r) U(r') e^{-|t-t'|\mu_b k_B T k^2 + i\mathbf{k} \cdot (\mathbf{r} + \mathbf{r}')} d\mathbf{r} d\mathbf{r}' d^3 \mathbf{k} \\
&= \frac{\mu_t^2 \rho}{(2\pi)^d} \iint \left[\frac{1 - 2q_\alpha^2}{p} e^{-\mathbf{q}^2} \right] \left(\frac{\pi}{p} \right)^{\frac{d}{2}} U(r) U(r') d\mathbf{r} d\mathbf{r}',
\end{aligned}
\tag{C12}
$$

where $p = |t - t'| \mu_b k_B T$, $\mathbf{q} = \frac{(\mathbf{r} + \mathbf{r}')}{2\sqrt{p}}$. When $|t - t'|$ is large enough, $\langle \eta_T^\alpha(0, t) \eta_T^\alpha(0, t') \rangle \propto |t - t'|^{-(d/2+1)}$.

---

[1] J. M. Berg, J. L. Tymoczko, and L. Stryer, *Kinesin and Dynein Move Along Microtubules*, in *Biochemistry* (W. H. Freeman, New York, 2002).

[2] N. Hirokawa, Y. Noda, Y. Tanaka, and S. Niwa, Kinesin superfamily motor proteins and intracellular transport, Nat. Rev. Mol. Cell Biol. **10**, 682 (2009).

[3] R. D. Vale, The molecular motor toolbox for intracellular transport, Cell **112**, 467 (2003).

[4] B. Milic, J. O. L. Andreasson, W. O. Hancock, and S. M. Block, Kinesin processivity is gated by phosphate release, Proc. Natl. Acad. Sci. USA **111**, 14136 (2014).

[5] M. Dogan, S. Can, F. Cleary, V. Purde, and A. Yildiz, Kinesin's front head is gated by the backward orientation of its neck linker, Cell Rep. **10**, 1967 (2015).

[6] H. Isojima, R. Iino, Y. Niitani, H. Noji, and M. Tomishige, Direct observation of intermediate states during the stepping motion of kinesin-1, Nat. Chem. Biol. **12**, 290 (2016).

[7] R. D. Vale and F. Oosawa, Protein motors and Maxwell's demons: Does mechanochemical transduction involve a thermal ratchet? Adv. Biophys. **26**, 97 (1990).

[8] M. Guo, A. Ehrlicher, M. Jensen, M. Renz, J. Moore, R. Goldman, J. Lippincott-Schwartz, F. Mackintosh, and D. Weitz, Probing the stochastic, motor-driven properties of the cytoplasm using force spectrum microscopy, Cell **158**, 822 (2014).

[9] B. Parry, I. Surovtsev, M. Cabeen, C. O'Hern, E. Dufresne, and C. Jacobs-Wagner, The bacterial cytoplasm has glass-like properties and is fluidized by metabolic activity, Cell **156**, 183 (2014).

[10] K. Nishizawa, M. Bremerich, H. Ayade, C. F. Schmidt, T. Ariga, and D. Mizuno, Feedback-tracking microrheology in living cells, Sci. Adv. **3**, e1700318 (2017).

[11] É. Fodor, M. Guo, N. S. Gov, P. Visco, D. A. Weitz, and F. van Wijland, Activity-driven fluctuations in living cells, Europhys. Lett. **110**, 48005 (2015).

[12] K. Shin, S. Song, Y. H. Song, S. Hahn, J.-H. Kim, G. Lee, I.-C. Jeong, J. Sung, and K. T. Lee, Anomalous dynamics of in vivo cargo delivery by motor protein multiplexes, J. Phys. Chem. Lett. **10**, 3071 (2019).

[13] T. Kurihara, M. Aridome, H. Ayade, I. Zaid, and D. Mizuno, Non-Gaussian limit fluctuations in active swimmer suspensions, Phys. Rev. E **95**, 030601(R) (2017).

[14] C. Esparza López, A. Théry, and E. Lauga, A stochastic model for bacteria-driven micro-swimmers, Soft Matter **15**, 2605 (2019).

[15] I. Zaid and D. Mizuno, Analytical Limit Distributions from Random Power-Law Interactions, Phys. Rev. Lett. **117**, 030602 (2016).

[16] Y. Shi, C. L. Porter, J. C. Crocker, and D. H. Reich, Dissecting fat-tailed fluctuations in the cytoskeleton with active micropost arrays, Proc. Natl. Acad. Sci. USA **116**, 13839 (2019).

[17] T. Ariga, K. Tateishi, M. Tomishige, and D. Mizuno, Noise-Induced Acceleration of Single Molecule Kinesin-1, Phys. Rev. Lett. **127**, 178101 (2021).

[18] T. Ariga, M. Tomishige, and D. Mizuno, Experimental and theoretical energetics of walking molecular motors under fluctuating environments, Biophys. Rev. **12**, 503 (2020).

[19] T. Ariga, M. Tomishige, and D. Mizuno, Nonequilibrium Energetics of Molecular Motor Kinesin, Phys. Rev. Lett. **121**, 218101 (2018).

[20] G. Paneru, J. T. Park, and H. K. Pak, Transport and diffusion enhancement in experimentally realized non-Gaussian correlated ratchets, J. Phys. Chem. Lett. **12**, 11078 (2021).

[21] Y. Ezber, V. Belyy, S. Can, and A. Yildiz, Dynein harnesses active fluctuations of microtubules for faster movement, Nat. Phys. **16**, 312 (2020).

[22] X.-L. Wu and A. Libchaber, Particle Diffusion in a Quasi-Two-Dimensional Bacterial Bath, Phys. Rev. Lett. **84**, 3017 (2000).

[23] M. J. Kim and K. S. Breuer, Enhanced diffusion due to motile bacteria, Phys. Fluids **16**, L78 (2004).

[24] K. C. Leptos, J. S. Guasto, J. P. Gollub, A. I. Pesci, and R. E. Goldstein, Dynamics of Enhanced Tracer Diffusion in Suspensions of Swimming Eukaryotic Microorganisms, Phys. Rev. Lett. **103**, 198103 (2009).

[25] C. Valeriani, M. Li, J. Novosel, J. Arlt, and D. Marenduzzo, Colloids in a bacterial bath: Simulations and experiments, Soft Matter **7**, 5228 (2011).

[26] S. A. Mallory, C. Valeriani, and A. Cacciuto, Curvature-induced activation of a passive tracer in an active bath, Phys. Rev. E **90**, 032309 (2014).

[27] C. Maggi, M. Paoluzzi, N. Pellicciotta, A. Lepore, L. Angelani, and R. Di Leonardo, Generalized Energy Equipartition in Harmonic Oscillators Driven by Active Baths, Phys. Rev. Lett. **113**, 238303 (2014).

[28] S. Krishnamurthy, S. Ghosh, D. Chatterji, R. Ganapathy, and A. Sood, A micrometre-sized heat engine operating between bacterial reservoirs, Nat. Phys. **12**, 1134 (2016).

[29] E. W. Burkholder and J. F. Brady, Tracer diffusion in active suspensions, Phys. Rev. E **95**, 052605 (2017).

[30] C. Maggi, M. Paoluzzi, L. Angelani, and R. Di Leonardo, Memory-less response and violation of the fluctuation-dissipation theorem in colloids suspended in an active bath, Sci. Rep. **7**, 17588 (2017).

[31] A. Suma, L. F. Cugliandolo, and G. Gonnella, Tracer motion in an active Dumbbell fluid, J. Stat. Mech. (2016) 054029.

[32] L. Dabelow, S. Bo, and R. Eichhorn, Irreversibility in Active Matter Systems: Fluctuation Theorem and Mutual Information, Phys. Rev. X **9**, 021009 (2019).

[33] P. Liu, S. Ye, F. Ye, K. Chen, and M. Yang, Constraint Dependence of Active Depletion Forces on Passive Particles, Phys. Rev. Lett. **124**, 158001 (2020).

[34] K. Kanazawa, T. G. Sano, A. Cairoli, and A. Baule, Loopy Lévy flights enhance tracer diffusion in active suspensions, Nature (London) **579**, 364 (2020).

[35] A. Lagarde, N. Dagès, T. Nemoto, V. Démery, D. Bartolo, and T. Gibaud, Colloidal transport in bacteria suspensions: From bacteria collision to anomalous and enhanced diffusion, Soft Matter **16**, 7503 (2020).

[36] O. Granek, Y. Kafri, and J. Tailleur, Anomalous Transport of Tracers in Active Baths, Phys. Rev. Lett. **129**, 038001 (2022).

[37] M. Rauscher, A. Domínguez, M. Krüger, and F. Penna, A dynamic density functional theory for particles in a flowing solvent, J. Chem. Phys. **127**, 244906 (2007).

[38] M. Baiesi, C. Maes, and B. Wynants, Fluctuations and Response of Nonequilibrium States, Phys. Rev. Lett. **103**, 010602 (2009).

[39] C. Maes, S. Safaverdi, P. Visco, and F. van Wijland, Fluctuation-response relations for nonequilibrium diffusions with memory, Phys. Rev. E **87**, 022125 (2013).

[40] J. R. Gomez-Solano, A. Petrosyan, S. Ciliberto, and C. Maes, Fluctuations and response in a non-equilibrium micron-sized system, J. Stat. Mech. (2011) P01008.

[41] M. Krüger and C. Maes, The modified Langevin description for probes in a nonlinear medium, J. Phys.: Condens. Matter **29**, 064004 (2017).

[42] C. Maes, Fluctuating Motion in an Active Environment, Phys. Rev. Lett. **125**, 208001 (2020).

[43] C. Maes, Response theory: A trajectory-based approach, Front. Phys. **8**, 229 (2020).

[44] M. Feng and Z. Hou, Effective dynamics of tracer in active bath: A mean-field theory study, arXiv:2110.00279.

[45] V. Démery, O. Bénichou, and H. Jacquin, Generalized Langevin equations for a driven tracer in dense soft colloids: Construction and applications, New J. Phys. **16**, 053032 (2014).

[46] V. Démery and D. S. Dean, Perturbative path-integral study of active- and passive-tracer diffusion in fluctuating fields, Phys. Rev. E **84**, 011148 (2011).

[47] V. Démery and É. Fodor, Driven probe under harmonic confinement in a colloidal bath, J. Stat. Mech. (2019) 033202.

[48] O. Dauchot and V. Démery, Dynamics of a Self-Propelled Particle in a Harmonic Trap, Phys. Rev. Lett. **122**, 068002 (2019).

[49] V. Démery and D. S. Dean, Drag Forces in Classical Fields, Phys. Rev. Lett. **104**, 080601 (2010).

[50] A. Maitra and R. Voituriez, Enhanced Orientational Ordering Induced by an Active yet Isotropic Bath, Phys. Rev. Lett. **124**, 048003 (2020).

[51] I. Gazuz and M. Fuchs, Nonlinear microrheology of dense colloidal suspensions: A mode-coupling theory, Phys. Rev. E **87**, 032304 (2013).

[52] J. Reichert and T. Voigtmann, Tracer dynamics in crowded active-particle suspensions, Soft Matter **17**, 10492 (2021).

[53] D. S. Dean, Langevin equation for the density of a system of interacting Langevin processes, J. Phys. A: Math. Gen. **29**, L613 (1996).